Supplementary Information for "Beta-Band Oscillations without Pathways: the opposing Roles of D2 and D5 Receptors" by Jean F. Liénard, Ignasi Cos and Benoît Girard

Obtention of realistic axonal delays

Several experiments have been conducted to decipher the temporal dynamics of the primate BG. In particular, stimulation experiments elicit actions potentials in one population through a strong local excitation, and record the time needed for the perturbation flow to reach other nuclei. The resulting chains of observed excitations/inhibitions are caricatural, as the excitations often push the spiking capacities of neurons to their limits and as the inhibitions often result in a complete absence of spike (Nambu et al., 2000). In order to use them to find plausible axonal delay, we hence developed a simple model that allows the reproduction of these chains of excitations/inhibitions. Our methodology to include all the timing of stimulation experiments is a two-staged process.

First, the procedure consists of establishing a list of all the possible pathways that can be involved in the stimulation experiments (Section). In order to do this, we develop the graph of the projections potentially involved into series of candidate pathways. The interactions in the STN ↔ GPe are recursive and hence the number of pathways are infinite, but we can rule out all but a small number of them based on additional experimental evidence. We develop the different pathways until we can justify their non-involvement in the experiment, providing us a set of candidate pathways that are summarized along with the experimental timing references in Tables S1 and S2.

Second, we explore exhaustively the space of axonal delays in order to chose those that fit best to these data (Section). In order to achieve this, we compute the time that would be needed by each pathway in our simplistic model to match to the experimentally recorded delay, and score the fit of the quickest pathway with experimental data.

Pathways possibly involved in the stimulation experiments

Although the Str is recurrently interconnected with the STN and GPe, only the striatofugal efferents connections are powerful enough to be involved in the stimulation experiments (Fig. 2, b). Indeed, stimulations of the cortex elicit only an overactivity in the MSN of Str that is not followed by a noticeable second excitation (Nambu et al., 2002). Using *reductio ad absurdum*, we can establish that the GPe → MSN pathway is not recruited in the experimental stimulation, because if it were recruited then the subsequent inhibition of the GPe should in turn excite the MSN activity. Furthermore, excitation in the STN fails to elicit response in the MSN (Kita et al., 2005), so the STN → MSN is not to be recruited in stimulation experiments. Notice that the resulting simplification of the BG connectivity graph is also in line with the results of our previous study (Liénard and Girard, 2014) which showed that the influence of these pathways on the striatum could only be potent if they targetted the FSI. Hence, they could only influence the MSN by silencing them through interneurons, and as MSN are already mostly silent at rest, this should not have observable consequences on the other nuclei.

Stimulations in the cortex, Str, STN or GPe result in an intricate superposition of excitatory and inhibitory effects that could be supported by a multitude of different pathways. We can however simplify the connection graph to rule out several pathways. We will successively review the different stimulation locations, the excitatory or inhibitory responses that they cause and the pathways that could be mediating these responses.

First we considered the case of the striatal stimulation (Fig. S1). Following this stimulation, GPe and GPi neurons are first inhibited, then excited (Kita et al., 2006). The artificial blockade of STN eliminates the excitation but does not affect the inhibition (Kita et al., 2006), hence the STN is required for the excitation. The excitation can thus not possibly be mediated by the (Str → GPe → GPi) chain because it does not

involve the required STN, so we can rule out pathway number 1 of Fig. S1. Furthermore, the artificial blockade of STN does not change the timing of the inhibition, so we can also rule out the pathways number 2 and 3 of Fig. S1 because the chains (Str → GPe → STN → GPe → GPi) and (Str → GPe → STN → GPe → STN → GPe → GPi) involve the STN and result in an inhibition of GPi.
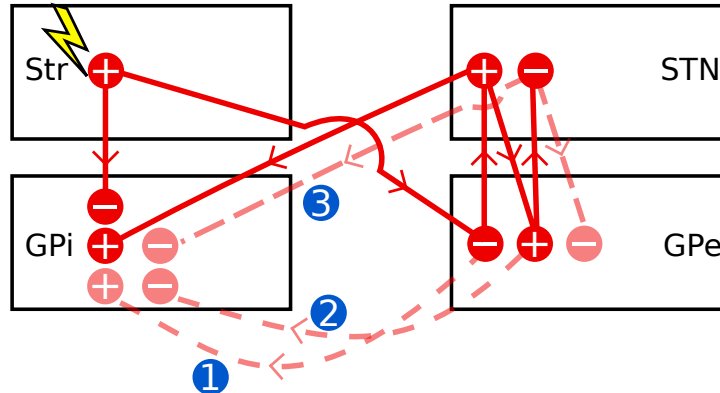

Figure S1: Possible timecourses of a striatal stimulation. A circled "+" denotes that the nucleus is overactive, while "-" denotes that it is underactive. Successive states of overactivity or underactivity are placed from left to right if they can be ordered (e.g. after an excitation in the Str, the STN will always be overactive before being underactive). Successive states that can not be ordered are placed on different lines (e.g. after an excitation in the Str, the first state of GPi could *a priori* be either an underactivity or an overactivity). Dashed numbered links correspond to pathways that are not recruited, see text for their individual justifications.

Next we considered a stimulation in the STN (Fig. S2). Following this, more than 80% of the responding neurons in the globus pallidus are excited (Nambu et al., 2000). As this excitation is not followed by an observable inhibition, we can rule out the pathways numbered 1, 2 and 3 of Fig. S2 because they would lead to an underactivity either in GPe or GPi.
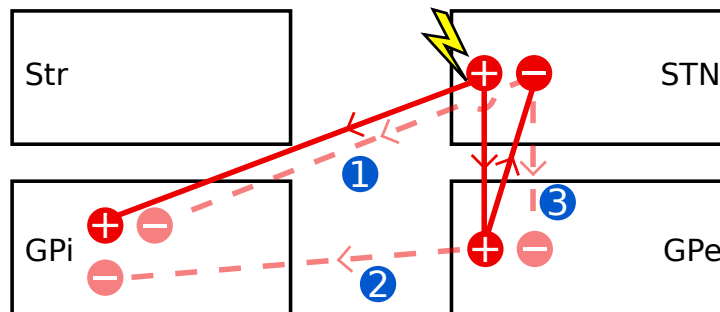

Figure S2: Possible timecourse of a stimulation in STN. See Fig. S1 for notations.

We then considered the GPe stimulation (Fig. S3). In this experiment, only half of the GPi neurons show an early excitation occuring fast (3.4 ± 0.9 ms), and they all show later an inhibition that is followed by an excitation (Tachibana et al., 2008). This early excitation can hardly be explained by the basal ganglia pathways, because the chains finishing earliest in the GPi, i.e. (GPe → STN → GPi) and (GPe → GPi), result in an inhibition. The (GPe → Str → GPi) chain could possibly account for this early excitation,

however we did not include the GPe → MSN pathway as it does not seem involved in these stimulation experiments (c.f. the beginning of this section), and furthermore the latency of this excitation is clearly too fast to be mediated through the slow Str → GPi connection. Finally, as discussed in Tachibana et al. (2008), the early excitation could be mediated by STN axons targeting both the GPe and GPi. As this does account for the fact that only half of GPi neurons respond and as other pathways can not plausibly explain an early excitation that is this fast, we will not consider further this early excitation. We can also rule out the pathways numbered 1 and 2 because they suppose a late inhibition following the reported inhibition and excitation in GPi, and Tachibana et al. (2008) did not report such a late inhibition.
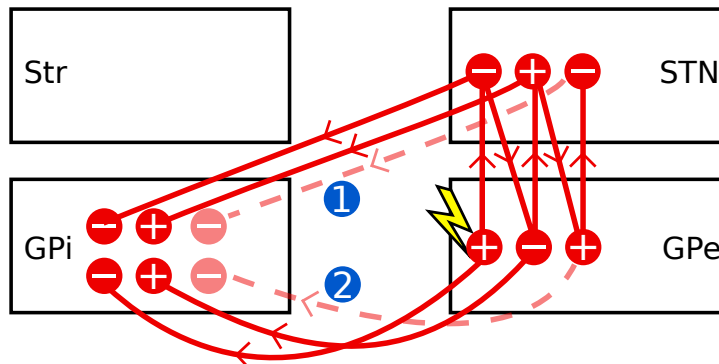

Figure S3: Possible timecourse of a stimulation in GPe. See Fig. S1 for notations.

Finally, Fig. S4 illustrates the case of the cortical stimulation. This stimulation leads to three distinct temporal responses in STN, GPe and GPi (Nambu et al., 2000): an early excitation followed by an inhibition, and finally a late excitation. To understand the possible timecourses of this cortical stimulation, we subdivided it according to the chains beginning with the direct striatal excitation (Fig. S4 left) and with the direct subthalamic excitation (Fig. S4 right). After the artificial blockade of activity in the STN, Nambu et al. (2000) reported that the GPi does not exhibit the early or late excitation. We can thus deduce that the STN is required for these excitations, so we can rule out the pathway 1 of Fig. S4 corresponding to the chain (Ctx → Str → GPe → GPi) because the STN is not involved in it. Nambu et al. (2000) also reports that after STN blockade, the GPi exhibits the same inhibition, so we deduce that the STN is not part of the chains leading to an inhibition in GPi and rule out the pathways 2 to 6, corresponding to the chains involving the STN and resulting in an underactivity in GPi. No late inhibition has been reported in Nambu et al. (2000), so the pattern of activity "-" then "+" then "-" in the STN is not plausible. We hence rule out the pathway 7.

Cost function to minimize

To compute the time t needed for the stimulation in "nucleus 1" to flow over a given chain (nucleus 1 → nucleus 2 → ... → nucleus n) and to be eventually recorded in "nucleus n", we use a simple formula:

$$t = \Phi + \sum_{i=1}^{n-1} (\delta_{i \to i+1} + \xi)$$

with $\delta_{i \to i+1}$ the axonal delay between nuclei i and $i+1$, Φ the time needed for the stimulation to be effective in nucleus 1 and ξ the time needed to any nucleus to change their firing rate when receiving the stimulation. The time required for the stimulation to be effectively eliciting action potentials is very small, so we set $\Phi = 1$ ms a value of $\Phi = 0$ ms was also considered and led to similar results). The time required for the action potential once at the synapse level to be captured by the postsynaptic neuron and to change its potential was considered to be $\xi = 1$ ms, equal for all populations for the sake of simplicity. This latter
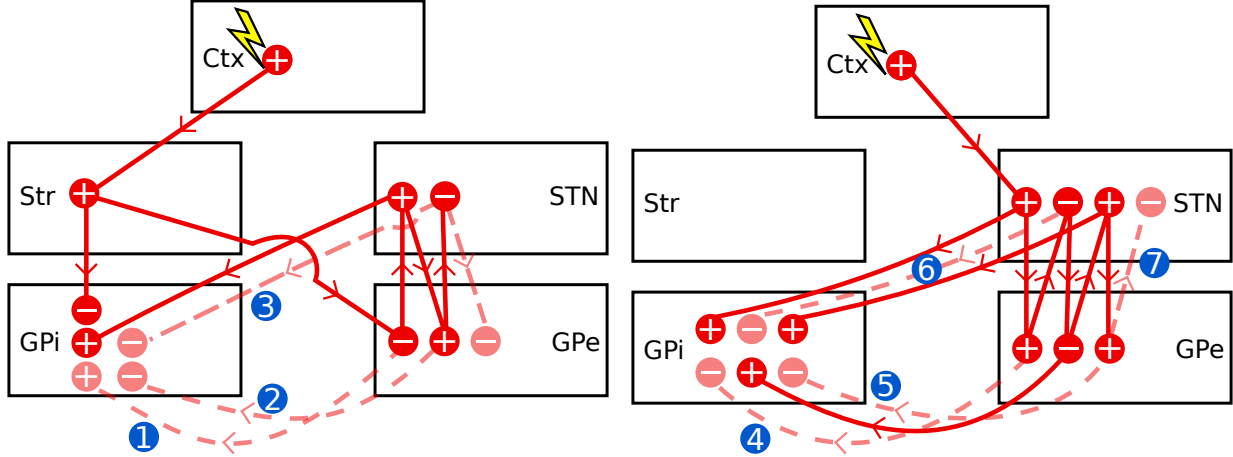
Figure S4: Possible timecourse of a cortical stimulation, which is subdivided for clarity into one representation of the striatal excitation consequences (left) and of the subthalamic excitation consequences (right). See Fig. S1 for notations.

constant is justified from the shape of the change of intensity after a spike mediated by either AMPA or $GABA_A$, because it is already significant after 1 ms (Destexhe et al., 1998) and this is in line with the alpha functions that we used in the BCBG model (Liénard and Girard, 2014).

As a general rule, each candidate pathway is computed for each response type, and the quickest pathway is assumed to be the one that we observe. The exceptions are the cortical stimulations as they cause an early and a late excitation, in these cases the quickest excitatory response is assumed to correspond to the early excitation and the quickest excitatory response *after the inhibition* is assumed to correspond to the late excitation. Overall, 18 pathways corresponding to 18 couples of (stimulation/response) are checked against 30 experimental data. These experimental data are noted as $T_{i,j} \pm \sigma_{i,j}$ with i the number of the (stimulation/response) pair and j the indice of the reference for each pair, as given in Tables S1 and S2. The global score χ of the fit between the timing of selected pathways and the reference data is then computed as:

$$\chi = \sum_{i=1}^{18} \left(\sum_j exp(\frac{-(t_i - T_{i,j})^2}{2\sigma_{i,j}^2}) \right)$$

The exhaustive search on axonal delays is conducted for every integer between 1 and 12 ms, as this upper bound can account for all the slowest direct responses recorded, including the Ctx $\rightarrow$ Str projection which takes around 8-10 ms (Nambu et al., 2000, Turner and DeLong, 2000) and Str $\rightarrow$ GPe/GPi which takes around 10-13 ms (Yoshida et al., 1993, Nambu et al., 2000). As 8 connections are considered (Fig. 2,b), the number of studied permutations rises to 12^8.

Timing data from literature review

The timing data used to compute the best set of transmission delays is summarized in Tables S1 and S2.

Stim.	Rec.	Response	Candidate pathways	Latency (ms)
Str	GPe	inhibition	Str → GPe	10.5 ± 3.2 [A] 10.4 ± 7.4 [B]
		excitation	Str → GPe → STN → GPe	26.5 ± 6.7 [A]
	GPi	inhibition	Str → GPi	13.1 ± 3.5 [A] 10.4 ± 7.4 [B]
		excitation	Str → GPe → STN → GPi	27.5 ± 6.7 [A]
STN	GPe	excitation	STN → GPe	5.5 ± 2.3 [C]
	GPi	excitation	STN → GPi	4.7 ± 1.9 [C]
GPe	GPi	inhibition	GPe → GPi GPe → STN → GPi	4.6 ± 1.1 [D]
		excitation	GPe → STN → GPe → GPi GPe → STN → GPe → STN → GPi	21.4 ± 8.6 [D]

[A]:Kita et al. (2006) [B]:Yoshida et al. (1993) [C]:Nambu et al. (2000) [D]:Tachibana et al. (2008)

Table S1: Summary of the candidate pathways and reference data in ms (Part 1). The column "Stim." indicates the location of the stimulation; "Rec." indicates the location of the recording; "Response" indicates the type of response recorded; the candidate pathways along the quantitative data expressed as mean±SD constitute the remainder of the table.

Stim.	Rec.	Response	Candidate pathways	Latency (ms)
Ctx	Str	excitation	Ctx → Str	10.2 ± 2.5 [A] 8.5 ± 5.9 [B]
	STN	early exc.	Ctx → STN	5.8 ± 2.6 [C] 6.5 ± 2.0 [D]
		inhibition	Ctx → Str → GPe → STN → GPe → STN Ctx → STN → GPe → STN	16.6 ± 6.9 [C]
		late exc.	Ctx → Str → GPe → STN Ctx → STN → GPe → STN → GPe → STN	32.3 ± 11.8 [C] 16.0 ± 2.8 [D]
	GPe	early exc.	Ctx → Str → GPe → STN → GPe Ctx → STN → GPe	9.2 ± 3.8 [C] 8.7 ± 1.3 [E]
		inhibition	Ctx → Str → GPe Ctx → STN → GPe → STN → GPe	16.9 ± 4.4 [C] 16.9 ± 2.0 [E]
		late exc.	Ctx → Str → GPe → STN → GPe Ctx → STN → GPe Ctx → STN → GPe → STN → GPe → STN → GPe	25.8 ± 2.6 [C] 30.8 ± 1.9 [E]
	GPi	early exc.	Ctx → Str → GPe → STN → GPi Ctx → STN → GPi Ctx → STN → GPe → STN → GPe → GPi	7.8 ± 2.4 [C] 9.2 ± 2.2 [F]
		inhibition	Ctx → Str → GPi	20.5 ± 3.1 [C] 19.4 ± 3.0 [F] 24.6 ± 5.1 [G]
		late exc.	Ctx → Str → GPe → STN → GPi Ctx → STN → GPi Ctx → STN → GPe → STN → GPe → GPi Ctx → STN → GPe → STN → GPe → STN → GPi	29.7 ± 2.9 [C] 32.6 ± 8.7 [F]

[A]:Nambu et al. (2002)   [B]:Turner and DeLong (2000)   [C]:Nambu et al. (2000)   [D]:Iwamuro et al. (2009)   [E]:Kita et al. (2004)
[F]:Tachibana et al. (2008)   [G]:Yoshida et al. (1993)

Table S2: Summary of the candidate pathways and reference data (Part 2). See Table S1 for notations.

Mathematical model

The structure of the model is very close to the one presented in Liénard and Girard (2014), with the exception of the addition of plausible axonal delays (detailed in section 2 of methods) and dopamine depletion (section 2). We use a population model with mean-field formulation. Although we provide here the basic equations of our model, more details about mean-field models can be found elsewhere (e.g. Deco et al., 2008).

One assumption of mean-field models, commonly referred as the *diffusion approximation*, is that every neuron receive the same inputs from another population. We can hence express the mean number of incoming spikes with neurotransmitter n per neuron of the population x from population y:

$$\Psi_x^n(t) = \nu_{i \leftarrow y} \phi_k(t - \tau_{y \rightarrow x}) \tag{3}$$

with $\nu_{x \leftarrow y}$ the mean number of synapse in one neuron of population x from axons of population y, $\tau_{y \rightarrow x}$ the axonal delay between population y and x, and $\phi_y(t - \tau_{y \rightarrow x})$ the firing rate of population y at time $t - \tau_{y \rightarrow x}$.

The axonal varicosity counts $\nu_{x \leftarrow y}$ is the mean count of synapses in population x that are targeted by axons from population y:

$$\nu_{x \leftarrow y} = \frac{\mathcal{P}_{y \rightarrow x} N_y}{N_x} . \alpha_{y \rightarrow x} \tag{4}$$

with N_x and N_y the neuron counts of populations x and y, $\alpha_{y \rightarrow x}$ the mean axonal varicosity count of neurons of y with an axon targeting neurons of x, and $\mathcal{P}_{y \rightarrow x}$ the proportion of such neurons in population y.

Mean-field models assume that neurons' firing thresholds follow a Gaussian distribution. The mean firing rate of a population x at time t can then be approximated by:

$$\phi_x(t) = \frac{S_x^{\max}}{1 + \exp(\frac{\theta_x - \Delta V_x(t)}{\sigma\prime})} \tag{5}$$

with $\Delta V_x(t)$ the mean input potential at the soma at time t, $S_x^{\max}$ the maximal possible firing rate, θ_x the mean difference between resting and firing thresholds, and, as per Van Albada and Robinson (2009), $\sigma\prime = \sigma \frac{\sqrt{3}}{\pi}$ (σ being the standard deviation of the firing thresholds).

The post-synaptic potential (PSP) change to the membrane potential at the location of the synapse contributed by a single spike is modeled by the alpha function (**?**):

$$V_0^n(t) = ADte^{-Dt} \tag{6}$$

where A and D relate to the amplitude and duration of PSP and depend on the neurotransmitter n mediating the spike. They are computed as follows: $A = A_n \, exp(1)$ and $D = \frac{exp(1)}{D_n}$ (Tsirogiannis et al., 2010), using the constants reported in Liénard and Girard (2014).

We also model in a simple way the attenuation of distal dendrites as a function of the soma distance. By modeling the dendritic field as a single compartment finite cable with sealed-end boundaries condition (Koch, 2005), we can express for population x:

$$V_{\text{soma}}^n(t) = V_0^n(t) \frac{cosh(L_x - Z_x)}{cosh(L_x)} \tag{7}$$

with $V_0^n(t)$ the potential change at the synapse, L_x the electrotonic constant of the neurons and Z_x the mean distance of the synaptic receptors along the dendrites. We further express this mean distance as a percentage of L_x: $Z_x = p_x L_x$. The electrotonic constant is then calculated according to (Koch, 2005):

$$L_x = l_x \sqrt{\frac{4}{d_x}\frac{R_i}{R_m}} \tag{8}$$

with R_i the intracellular resistivity, R_m the membrane resistance, l_x the mean maximal dendritic length and d_x the mean diameters of the dendrites along their whole extent for population x.

Finally, we express $\Delta V_x(t)$ the mean change of potential of one population caused by all its afferents:

$$\Delta V_x(t) = \sum_{(y,n)} \Psi_x^n(t) V_{\text{soma}}^n(t) \tag{9}$$

with each couple (y, n) representing one afferent population y whose spikes are mediated by a neurotransmitter n.

The BG dynamics were simulated with a time-step of 10^{-4} ms, as in Liénard and Girard (2014), using a 4th order Runge-Kutta integration method. The code of the model is available on ModelDB under the accession number 150206 and on github at https://github.com/jealie/BCBG-model.

9

Activity of BG nuclei following DA depletion, and with striato-pallidal and striato-subthalamic feedback loops selectively deactivated
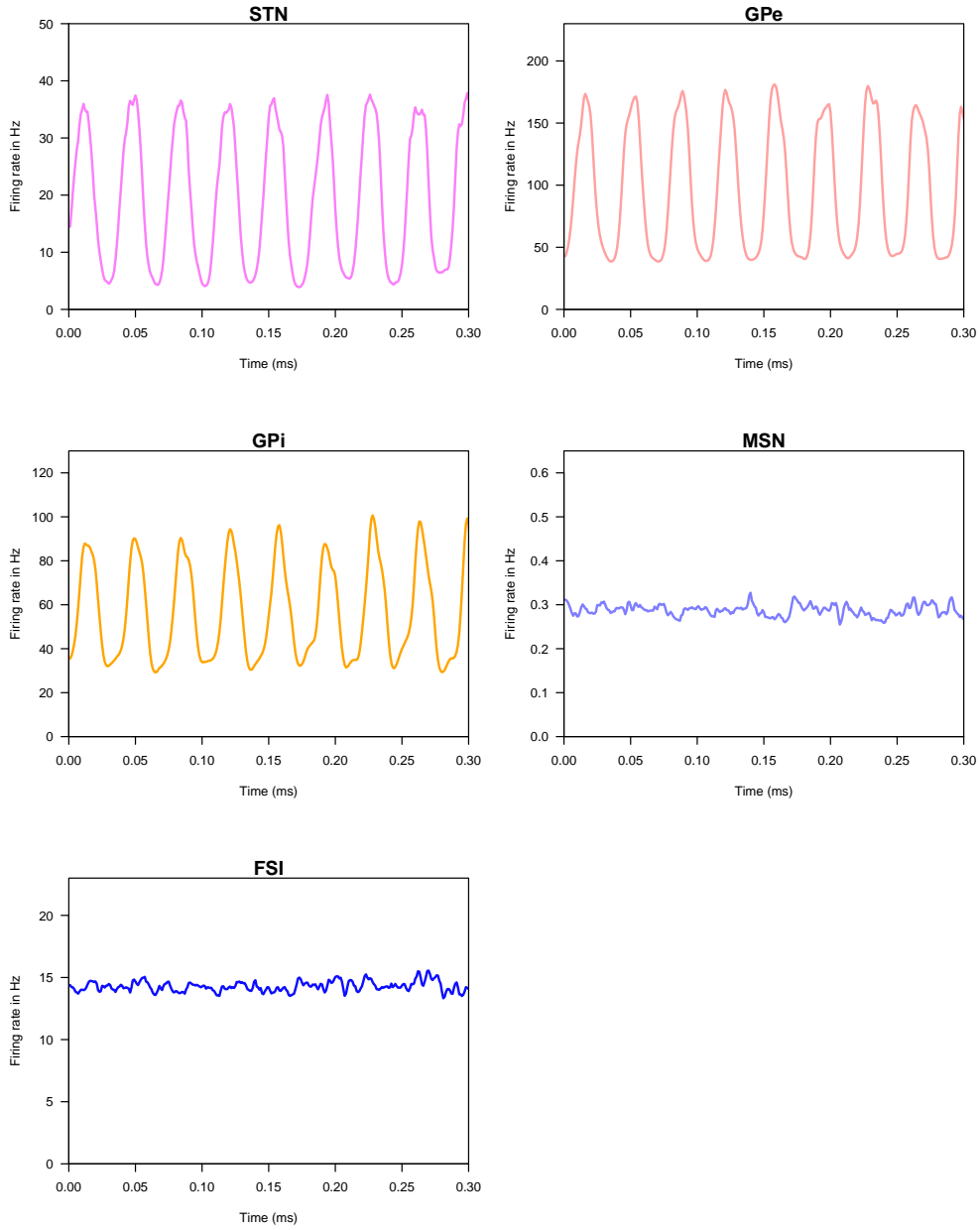

Figure S5: This figure shows the activities of all nuclei under dopamine depletion, as Fig. 3 in main text. However, in this simulation all pallidostriatal and subthalamostriatal feedback were overridden: instead of being driven by the oscillating neuronal activity, these afferents to striatum were simulated as if GPe and STN activity was at its normal level. Oscillations in MSN and FSI disappear, demonstrating that striatal oscillations are byproduct of GPe-STN oscillations in our model.
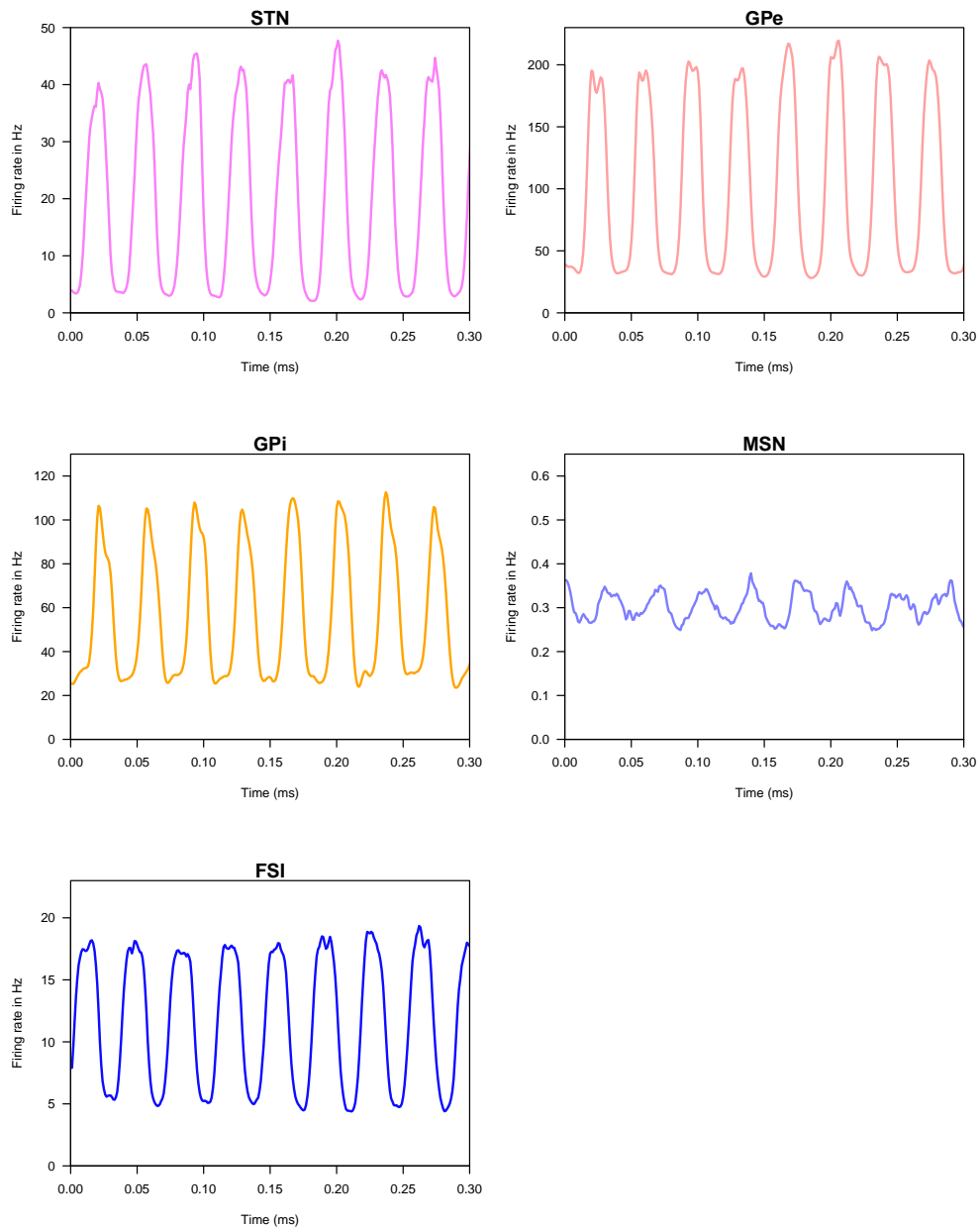
Figure S6: Activities of all individual nuclei with only the GPe → FSI feedback enabled. Weak oscillatory behavior is visible in the MSN activity, demonstrating that striatal oscillations are mediated by the pallido-FSI connections and thus ultimately driven by the GPe.

References

Deco, G., Jirsa, V., Robinson, P., Breakspear, M., and Friston, K. (2008). The dynamic brain: from spiking neurons to neural masses and cortical fields. *PLoS Computational Biology*, 4(8):e1000092.

Destexhe, A., Mainen, Z., and Sejnowski, T. (1998). Kinetic models of synaptic transmission. *Methods in Neuronal Modeling*, 2:1–25.

Iwamuro, H., Tachibana, Y., Saito, N., and Nambu, A. (2009). Organization of motor cortical inputs to the subthalamic nucleus in the monkey. *The Basal Ganglia IX*, pages 109–117.

Kita, H., Chiken, S., Tachibana, Y., and Nambu, A. (2006). Origins of gabaa and gabab receptor-mediated responses of globus pallidus induced after stimulation of the putamen in the monkey. *The Journal of Neuroscience*, 26(24):6554–6562.

Kita, H., Nambu, A., Kaneda, K., Tachibana, Y., and Takada, M. (2004). Role of ionotropic glutamatergic and gabaergic inputs on the firing activity of neurons in the external pallidum in awake monkeys. *Journal of Neurophysiology*, 92(5):3069–3084.

Kita, H., Tachibana, Y., Nambu, A., and Chiken, S. (2005). Balance of monosynaptic excitatory and disynaptic inhibitory responses of the globus pallidus induced after stimulation of the subthalamic nucleus in the monkey. *The Journal of Neuroscience*, 25(38):8611–8619.

Koch, C. (2005). *Biophysics of computation: information processing in single neurons*. Oxford University Press, USA.

Liénard, J. and Girard, B. (2014). A biologically constrained model of the whole basal ganglia addressing the paradoxes of connections and selection. *Journal of Computational Neuroscience*, 36(3):445–468.

Nambu, A., Kaneda, K., Tokuno, H., and Takada, M. (2002). Organization of corticostriatal motor inputs in monkey putamen. *Journal of Neurophysiology*, 88(4):1830–1842.

Nambu, A., Tokuno, H., Hamada, I., Kita, H., Imanishi, M., Akazawa, T., Ikeuchi, Y., and Hasegawa, N. (2000). Excitatory cortical inputs to pallidal neurons via the subthalamic nucleus in the monkey. *Journal of Neurophysiology*, 84(1):289–300.

Tachibana, Y., Kita, H., Chiken, S., Takada, M., and Nambu, A. (2008). Motor cortical control of internal pallidal activity through glutamatergic and gabaergic inputs in awake monkeys. *European Journal of Neuroscience*, 27(1):238–253.

Tsirogiannis, G., Tagaris, G., Sakas, D., and Nikita, K. (2010). A population level computational model of the basal ganglia that generates parkinsonian local field potential activity. *Biological Cybernetics*, 102(2):155–176.

Turner, R. and DeLong, M. (2000). Corticostriatal activity in primary motor cortex of the macaque. *The Journal of Neuroscience*, 20(18):7096–7108.

Van Albada, S. and Robinson, P. (2009). Mean-field modeling of the basal ganglia-thalamocortical system. I Firing rates in healthy and parkinsonian states. *Journal of Theoretical Biology*, 257(4):642–663.

Yoshida, S., Nambu, A., and Jinnai, K. (1993). The distribution of the globus pallidus neurons with input from various cortical areas in the monkeys. *Brain Research*, 611(1):170–174.